Chracterization of Deformation in Injection Molded Parts after Packing and Cooling

Jung Hoon Jung, Seok Won Lee, Jae Ryoun Youn*

Department of Fiber and Polymer Science, Seoul National University, 56-1, Shinlim-dong, Kwanak-gu, Seoul, Korea

SUMMARY : Residual stresses which are developed in injection molded parts affect dimensional accuracy and mechanical properties of the final products. To predict the residual stresses in injection molded parts, three stages of injection molding, i. e., filling, packing, and cooling, must be taken into consideration for the thermal and flow analyses. Flow field anaysis for filling and postfilling stages has been carried out by using the control volume based FEM/FDM hybrid method. The generalized Hele-Shaw flow is assumed. Compressibility of the polymer melt is considered during packing and cooling stages. Modified Cross model is employed to reflect the dependency of the viscosity upon shear rate and temperature. An equation of state proposed by Tait offers an efficient means to describe *pvt*-relationship of the polymer. Variations in temperature and pressure fields are obtained over all stages by the numerical flow analysis and used as input data for the stress analysis of the part. Plane stress elements, such as shell elements, are used for finite element stress analysis of injection molded parts with appropriate boundary conditions both in the mold and after ejected from the mold. The numerical analysis yields useful information which is relevant to the mechanical properties of the final products, e. g., residual stress distribution, shape of deformation, displacement field, and strain distribution.

Introduction

Injection molding, a highly productive manufacturing process, is capable of producing intricate net shapes and thus is one of the most widely used processes for polymer processing. Recently, it is applied to processing of pure polymers, short fiber reinforced composites, and powder materials. Ceramic and metallic powders mixed with polymeric binders are injection molded to make precision parts. The binders are removed from the molded parts and the molded powder parts are sintered to increase the strength. Injection molding is a cyclic process which is composed of three stages, filling, packing, and cooling. Length of each cycle depends upon pressure and temperature variations in the cavity.

Polymer melt which is injected into the cavity experiences various deformations through the three stages. In the filling stage, the polymer melt flows into the arbitrary shaped cavity and is cooled by the relatively cold cavity wall while transition of the melt from liquid to solid state takes place causing molecular orientation. In the packing stage, high pressure is

 CCC 1022-1360/99/$ 17.50+.50/0

maintained to compensate the shrinkage of the polymer melt. Additional amount of polymer melt is packed into the cavity and residual flow is induced inside the cavity due to compressibility of the polymer melt and elastic deformation of the mold. Since the polymer melt is solidified by the heat transfer through the wall while it is being compressed, molecular orientation, crystallization, shrinkage, and warpage may be caused by the residual flow. The injected polymer parts are cooled inside the cavity after the gate is sealed and the packing pressure is removed. Through the three stages, residual stresses are developed and affect the dimensional accuracy and final properties of the product. To predict the deformation and dimensional accuracy of the injected part, all three stages must be considered for flow analysis.

Both experimental and numerical studies have been accomplished by many researchers to analyze injection molding process. In the numerical study, analysis of the filling stage was the most frequently studied topic. The numerical modeling of injection mold filling with arbitrary shaped planar cavity was developed by Hieber and Shen[1]. Postfilling stages have been investigated separately from the filling stages. In the investigation of postfilling stages, relations between applied packing pressure and deformation of the final part have been focused. Spencer and Gilmour[2] investigated the compressibility of the polymer melt to understand postfilling stages. Recently, Chiang et al.[3,4] developed a unified method which models both filling and postfilling stages continuously. In most investigations on residual stresses of injection molded parts, residual stresses are measured experimentally and final properties of the product are predicted by theoretical modeling based on the experimental results[5-7]. There have been only a few investigations on prediction of residual stresses by considering flow and stress analyses at the same time. Jansen and Titomanlio[8,9] proposed a model in which stress analysis is coupled with flow analysis. Chang and Tsaur[10] performed a stress analysis using flow analysis results considering the effect of crystallization, but their studies are limited to a geometrically simple mold.

In this paper, a unified flow analysis of filling and postfilling stages is carried out and residual stresses and final deformation of the molded part are predicted based on the flow analysis results. An elastic stress analysis is performed to predict deformation and residual stresses of the molded part after ejection by utilizing pressure and temperature data obtained from the flow analysis. To analyze the flow field in both filling and postfilling stages, the G.H.S. (Generalized Hele-Shaw) model, which represents non-isothermal, compressible, and viscous flow, proposed by Chiang[3] is used.

Modeling of Non-isothermal Compressible Flow

Governing Equation

Most injection-molded products have three dimensional and complex shapes. When considering local geometry, thickness of the part is much smaller than the characteristic length in plane. Since the flow at an arbitrary point inside the cavity is influenced by the local geometry, the polymer melt will flow in plane direction rather than thickness direction. The generalized Hele-Shaw approximation can be applied to the injection molding due to high viscosity of the polymer melt injected into the cavity and due to the assumption of planar flow. While the polymer melt is usually regarded as an incompressible fluid in previous studies[11,12], compressibility of the polymer melt is considered in this paper. By considering compressibility of the fluid, secondary flow due to high pressure in the packing stage can be predicted.

If the two dimensional planar flow inside the cavity is taken into account (Fig. 1), continuity equation can be represented as Eq. (1) in rectangular coordinates when considering the compressibility of polymer melt and neglecting velocity in thickness direction. Momentum equations in x, y directions are given by Eq. (2) and (3). Energy equation neglecting planar heat conduction and gapwise heat convection can be expressed as Eq. (4).

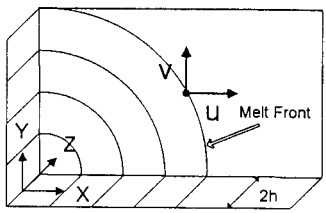

Fig. 1: Schematic description of melt flow in plane direction with the coordinate system employed.

$$\frac{\partial \rho}{\partial t}+\frac{\partial}{\partial x}(\rho u)+\frac{\partial}{\partial y}(\rho v)=0 \qquad 1$$

$$\frac{\partial}{\partial z}\left(\eta\frac{\partial u}{\partial z}\right)=\frac{\partial P}{\partial x} \qquad 2$$

$$\frac{\partial}{\partial z}\left(\eta\frac{\partial v}{\partial z}\right)=\frac{\partial P}{\partial y} \qquad 3$$

$$\rho C_p(T)\left(\frac{\partial T}{\partial t}+u\frac{\partial T}{\partial x}+v\frac{\partial T}{\partial y}\right)=\frac{\partial}{\partial z}\left(k(T)\frac{\partial T}{\partial z}\right)+\eta\dot{\gamma}^2 \qquad 4$$

where t is time, ρ is density as a function of pressure and temperature, x and y are planar coordinates, z is the coordinate in thickness direction, u and v are planar velocity components, P is pressure, η is non-Newtonian viscosity as a function of pressure, temperature, and magnitude of shear strain rate, $\dot{\gamma}$, T is temperature, $C_p(T)$ is heat capacity, and $k(T)$ is thermal conductivity. Boundary conditions needed to solve the governing equations are assumed as

$$u = v = 0 \ , \ T = T_w \qquad \text{at } z = h \qquad \textbf{5}$$

$$\frac{\partial u}{\partial z} = \frac{\partial v}{\partial z} = 0 \ , \ \frac{\partial T}{\partial z} = 0 \qquad \text{at } z = 0 \qquad \textbf{6}$$

where T_w is mold wall temperature, and h is half cavity thickness.

Planar velocities are obtained by integrating Eq. (2) and (3) using boundary conditions, (5) and (6). Mass flow rates per unit length in the x and y direction, $\dot{m}_x$ and $\dot{m}_y$ are obtained as below.

$$\dot{m}_x = 2\int_0^h \rho u \, dz \equiv -2\tilde{S}\frac{\partial P}{\partial x} \qquad \textbf{7}$$

$$\dot{m}_y = 2\int_0^h \rho v \, dz \equiv -2\tilde{S}\frac{\partial P}{\partial y} \qquad \textbf{8}$$

$$\tilde{S} \equiv \int_0^h \rho \int_z^h \frac{\tilde{z}}{\eta} \, d\tilde{z} \, dz \qquad \textbf{9}$$

where $\tilde{S}$ is a measure of fluidity considering density change, which is similar to the flow conductance used by Hieber and Shen[1]. Although calculation of flow conductance is simpler in the references [12] and [13] by neglecting density gradients in planar direction, formulation proposed by Chiang et al.[3] is adopted in this study to consider the density gradient in thickness direction.

Integration of Eq. (1) and substitution of Eq. (7) and (8) results in

$$2\frac{\partial}{\partial t}\int_0^h \rho \, dz + \frac{\partial}{\partial x}(\dot{m}_x) + \frac{\partial}{\partial y}(\dot{m}_y) = 0 \qquad \textbf{10}$$

Using chain rule and considering discontinuity of density at the interface between liquid and solid phases, Eq. (10) becomes

$$G\frac{\partial P}{\partial t} - \frac{\partial}{\partial x}\left(\tilde{S}\frac{\partial P}{\partial x}\right) - \frac{\partial}{\partial y}\left(\tilde{S}\frac{\partial P}{\partial y}\right) = -F \qquad \textbf{11}$$

where $$G = \int_0^x \left(\frac{\partial \rho_l}{\partial P}\right)_T dz + \int_x^h \left(\frac{\partial \rho_s}{\partial P}\right)_T dz \qquad \textbf{12}$$

$$F = \int_0^{\chi} \left(\frac{\partial \rho_l}{\partial T} \right)_P \frac{\partial T}{\partial t} dz + \int_{\chi}^{h} \left(\frac{\partial \rho_s}{\partial T} \right)_P \frac{\partial T}{\partial t} dz + (\rho_l - \rho_s)_{z=\chi} \frac{\partial \chi}{\partial t} \qquad \textbf{13}$$

ρ_l and ρ_s are densities of liquid and solid phases respectively, and χ is interface location. χ is the location of density discontinuity and considered only for semi-crystalline polymers. The last term in Eq. (13) represents abrupt change in density at the transition temperature and can be deleted in the case of amorphous polymers.

Splitting the first term in Eq. (10) into G and F terms as shown in Eq. (11) has a numerical advantage compared with treating it as a force vector[3]. The time derivative of the pressure in the first term makes Eq. (11) more implicit and enhances numerical stability. While the contribution of G and F terms to the numerical calculation is negligible in the filling analysis, G and F terms show dominant effects on the postfilling analysis because the value of $\tilde{S}$ approaches zero. During the filling stage, local packing effects are imposed as a result of early filling of some parts of the cavity. This phenomenon is also taken into account by calculation of G and F terms. Thus, splitting the first term as shown in Eq. (11) is necessary for the numerical stability and unified formulation of the filling and postfilling stages.

To solve Eq. (11), suitable boundary conditions are needed. Pressure is zero at the melt front and there is no flow across the mold wall.

$$P = 0 \qquad \text{at } C_m \qquad \textbf{14}$$

$$\frac{\partial P}{\partial n} = 0 \qquad \text{at } C_i \text{ or } C_o \qquad \textbf{15}$$

where C_m denotes the location of melt front, C_i the location of inserts, C_o the location of outer contour, and n the outward normal to the boundary. In addition, pressure of the polymer melt at the entrance into the cavity (e.g., at the gate or at the end of sprue) should be specified.

$$P = P_e(t) \qquad \text{at } C_e \qquad \textbf{16}$$

where C_e denotes the entrance region of the cavity. These geometrical boundaries are shown schematically in Fig. 2.

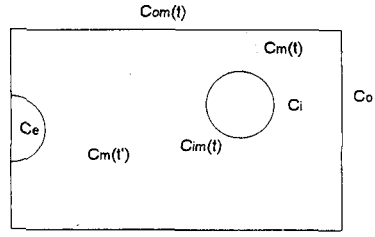

Fig. 2: Schematic expression of boundaries in the cavity.

In the injection molding process, pressure at the gate is influenced by the size of the mold,

the type of polymer used, and processing variables and varies with respect to time. Since it is difficult to predict pressure variation at the entrance to the cavity, a constant volume flow rate is assumed and the pressure is calculated to satisfy the constant flow rate condition.

When temperature distribution is predicted by solving Eq. (4), no boundary conditions in the planar direction are imposed because planar thermal conduction is neglected. Temperature at the melt front in the filling stage is assumed to be the same as that at the center right behind the melt front, which reflects fountain flow effect. Temperature at each gate is set to be the same as the inlet barrel temperature.

Tait equation is used as the state equation which can depict the density variation through liquid and solid phases[3].

$$v(P,T) = v_0(T)\left[1 - C\ln\left(1 + \frac{P}{B(T)}\right)\right] \qquad \textbf{17}$$

where

$$v_0(T) = \begin{cases} b_{1,l} + b_{2,l}\overline{T} & (T > T_t) \\ b_{1,s} + b_{2,s}\overline{T} & (T < T_t) \end{cases} \qquad \textbf{18}$$

$$B(T) = \begin{cases} b_{3,l}\exp(-b_{4,l}\overline{T}) & (T > T_t) \\ b_{3,s}\exp(-b_{4,s}\overline{T}) & (T < T_t) \end{cases} \qquad \textbf{19}$$

$$\overline{T} \equiv T - b_5 \qquad \textbf{20}$$

$$T_t(P) = b_5 + b_6 P \qquad \textbf{21}$$

$$C = 0.0894 \qquad \textbf{22}$$

$v(P,T)$ is the specific volume, T_t is transition temperature between solid and liquid phase, b_i's are material constants.

Modified Cross model is employed as the viscosity model to consider its dependence on magnitude of the shear strain rate, pressure, and temperature.

$$\eta = \frac{\eta_0}{1 + \left[\frac{\eta_0 \dot{\gamma}}{\tau^*}\right]^{1-n}} \qquad \textbf{23}$$

$$\eta_0 = B\exp\left(\frac{T_b}{T}\right)\exp(\beta P) \qquad \textbf{24}$$

where η_0 is zero-shear viscosity and shows Arrhenius type dependence on the pressure and temperature. B, T_b, β, τ^*, and n are material constants. The viscosity model and state equation are used for the solution of Eq. (11). The following model using 5 constants is used to determine heat capacity and thermal conductivity as a function of temperature when the energy equation is solved numerically.

$$C_p(T) = c_1 + c_2\tilde{T} + c_3 \tanh(c_4\tilde{T}) \qquad 25$$

$$k(T) = \lambda_1 + \lambda_2 T + \lambda_3 \tanh(\lambda_4 T) \qquad 26$$

where $\tilde{T} = (T - c_5)$, $T = (T - \lambda_5)$, and c_i's and λ_i's are material constants.

Pressure and velocity fields in the cavity are governed by Eq. (11) and the temperature distribution is obtained by Eq. (4). To make the numerical simulation more complete, flow and heat transfer in the sprue and runner should be considered. To accomplish this, one dimensional momentum and heat transfer equation based on cylindrical coordinates are derived and used for the numerical simulation.

Numerical Implementation

Finite element and finite difference methods are applied to the numerical analysis of flow and temperature fields using the governing equations. Three noded linear triangular elements are used for the prediction of pressure field in the cavity and linear tubular elements in the runner. Finite difference grids for the analysis of temperature field are distributed with uniform distance in the thickness direction for the triangular element and in radial direction for the tubular element (Fig. 3). Governing equations are non-linear and strongly coupled

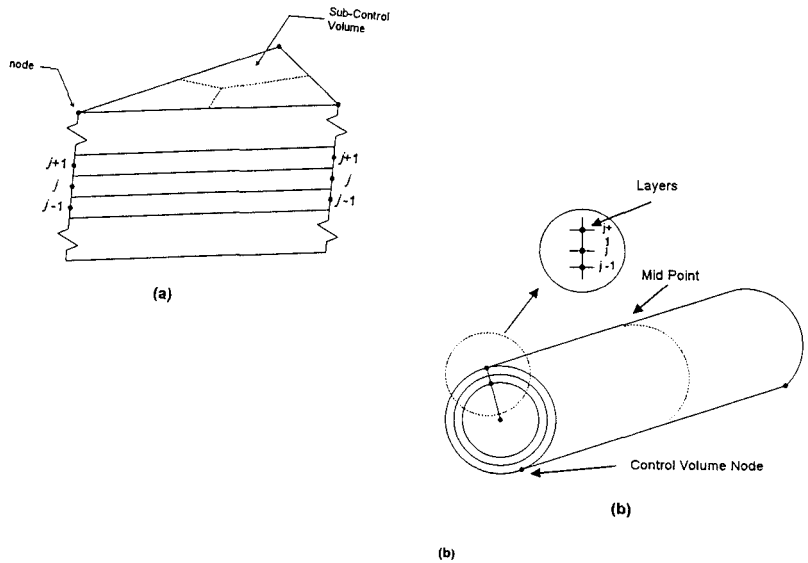

(b)

Fig. 3: Schematic diagram of (a) linear triangular finite elements and finite difference grids in thickness direction and (b) linear tubular finite elements and finite difference grids in radial direction.

each other. In addition, the boundary is moving with respect to time as melt front advances. To overcome difficulties in dealing with the moving boundary, melt front is advanced by the use of control volume approach and iteration for the pressure and temperature is performed in each time step.

Residual Stress Analysis

Polymeric melts deform into the desired shape during injection molding. Thereafter, the desired shape experiences cooling under high pressure. Especially in the injection molding process, applied pressure of more than 10 MPa (about 100 atm) and rapid cooling of the mold are required for high productivity. In addition, the polymer melt experiences various deformations in a complex-shaped cavity. The polymer product may deform as the residual stresses are developed due to non-uniform pressure and temperature fields during solidification. Residual stresses developed may cause dimensional inaccuracy and affect mechanical properties when external stresses are applied to the product. Generation of residual stresses can be explained both microscopically and macroscopically. In a microscopic point of view, the polymer melt experiences local stresses due to flow into the cavity during filling and postfilling stages, and molecular orientation and/or crystallization will occur. This molecular structure is likely to be frozen in the solid phase due to rapid cooling and results in local anisotropic shrinkage. In a macroscopic point of view, the product which is processed under high temperature and pressure experiences locally non-uniform temperature and pressure variations through the cooling stage and various internal thermal stresses are developed. Before ejection, these stresses are constrained by the mold, but, after ejection, geometric restrictions are removed for residual strains to develop. Jansen and Titomanlio[8,9] established a model that could calculate residual stresses of injection molded part incorporating above mentioned features, but they did not couple residual stress analysis and thermal flow analysis. Chang and Tsaur[10] made an attempt to couple these analyses considering the effect of crystallization, but their work was confined in a relatively simple geometry.

In this study, coupling between residual stress analysis and complex thermal flow analysis is attempted by using a simple assumption that only the thermal contraction causes residual stresses once the polymer is solidified. Thermal expansion coefficient is obtained from Tait's state equation as a function of pressure and temperature. Thus, the effect of pressure on the thermal expansion coefficient can be considered. It is assumed that no residual stress exists

above the glass transition temperature and solid state polymer is elastic. A thermoelastic stress analysis is performed using pressure and temperature distribution obtained from the thermal flow analysis. The finite element meshes used in the thermal flow analysis are used for the thermal stress analysis and plane stress is assumed to calculate residual stress and strain fields.

The thermal expansion coefficient, α, for an isotropic solid is defined as

$$\alpha = \frac{1}{3V}\frac{\partial V}{\partial T} \qquad \textbf{27}$$

where V is volume. Substitution of the relation between volume and specific volume ($V = mv$) results in

$$\alpha = \frac{1}{3v}\frac{\partial v}{\partial T} \qquad \textbf{28}$$

Thermal expansion coefficient is obtained from Tait's equation as a function of pressure and temperature.

$$\alpha = \frac{1}{3}\left\{\frac{\dfrac{C}{B(T)}\dfrac{PB'(T)}{B(T)+P}}{1-C\ln\left(1+\dfrac{P}{B(T)}\right)} + \frac{1}{v_0}\frac{\partial v_0}{\partial T}\right\} \qquad \textbf{29}$$

Estimation of the thermal expansion coefficient under various pressure and temperature is done by using the above equation (29) and the estimated values are applied to the thermal stress analysis.

Pressure and temperature fields are obtained as the result of non-isothermal compressible flow analysis for every nodal point from the beginning of filling to the end of cooling. The output data on pressure and temperature just before ejection are used as the initial condition for the thermal stress analysis. In injection molding, the polymer melt cools down below the glass transition temperature before ejection and thermal stresses begin to develop. Thermal stresses within the molded part are calculated after it cools below the glass transition temperature. Displacement boundary conditions are assigned in two steps; before ejection, displacements are assigned to be zero along the cavity wall, and after ejection, free boundary conditions are applied. Calculation is terminated when temperatures of all nodal points reach room temperature. A solid state stress analysis is performed by using a commercial FEM package, ABAQUS.

Results and Discussion

A numerical analysis is executed to investigate deformation and residual stress distribution of the injection molded parts by using finite element and finite difference methods. Three different cases shown in Fig. 4 are examined. The thickness of the cavity is 0.2 cm and the length and radius of the gate with circular cross-section are 0.35 cm and 0.075 cm respectively. Each circular runner has the radius of 0.3 cm.

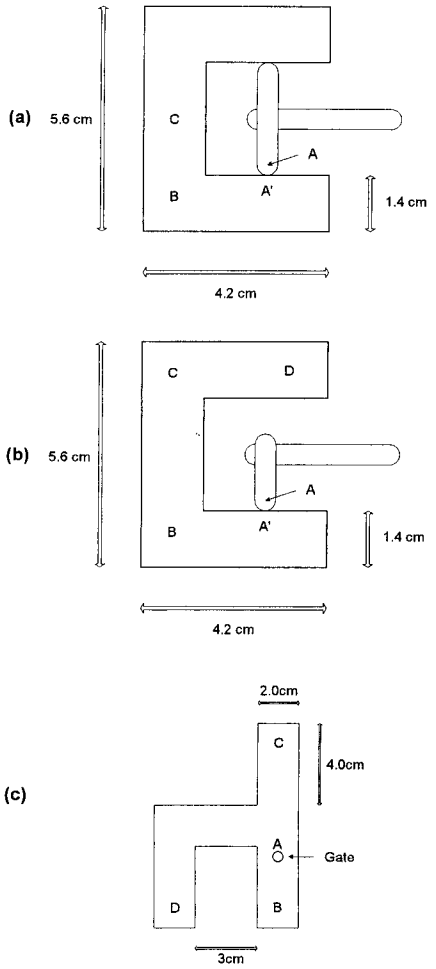

Fig. 4: Molds used for numerical analysis ; (a) mold A, (b) mold B, (c) mold C.

In mold A, gates are located in the opposite position so that the weld line will be formed at the center of the part. In mold B, there is only one gate so that the flow path may be longer than the case of mold A. Mold C has a somewhat complicated shape and the gate at point A as shown in Fig. 4. Processing conditions applied to each mold are given in Table 1.

Table 1. Processing conditions used in the flow field analysis for each mold.

	Q (cm^3/sec)	T_w (°C)	P_{pack} (MPa)	t_{eject} (sec)
Mold A	10.0	40.0	41.34	10.25
Mold B	10.0	40.0	41.34	10.28
Mold C	28.0	40.0	41.34	9.18

In mold A and B, processing conditions are the same, but gate and runner systems are different in order to show the effects of mold design on the final deformation of the product. In mold C, pressures and temperatures will be examined at different positions which have different flow paths and residual stresses. Diameter of the gate is assumed to be smaller than the thickness of the cavity or the diameter of the runner.

Polystyrene(PS) is selected as the molded material. Constants for the Tait's equation are given in Table 2 and constants for the viscosity model are given as n=0.274, τ^*=3.04×10^{-7} N/m^3, B=1330 Pa·sec, T_b=2.31×10^5 K, β=3.5×10^{-8} m^2/N. Constants for the specific heat and thermal conductivity are given in Table 3. Values of elastic modulus, E, and Poisson's ratio, ν, used in the analysis are given as E=3200 MPa, ν=0.32.

Table 2. Constants for Tait's model for polystyrene (ref. 4).

	constant	value		constant	value
$b_{1,l}$	(cm^3/g)	0.988	$b_{1,s}$	(cm^3/g)	0.988
$b_{2,l}$	(cm^3/gK)	6.10×10^{-4}	$b_{2,s}$	(cm^3/gK)	1.49×10^{-4}
$b_{3,l}$	(dyne/cm^2)	115.0×10^7	$b_{3,s}$	(dyne/cm^2)	238.0×10^7
$b_{4,l}$	(K^{-1})	3.66×10^{-3}	$b_{4,s}$	(K^{-1})	2.10×10^{-3}
b_5	(K)	385.0	b_6	(Kcm^2/dyne)	7.8×10^{-7}

Table 3. Constants for specific heat and thermal conductivity models for polystyrene.

	constant	value		Constant	value
c_1	(erg/g°C)	1.55×10^7	λ_1	(erg/cm°Csec)	1.49×10^4
c_2	(erg/g°C^2)	2.99×10^4	λ_2	(erg/cm°C^{2}sec)	16.31
c_3	(erg/g°C)	1.74×10^6	λ_3	(erg/cm°Csec)	0.0
c_4	(°C^{-1})	6.68×10^{-2}	λ_4	(°C^{-1})	0.0
c_5	(°C)	79.6	λ_5	(°C)	100.0

Mold A

Pressure variations at four different points shown in Fig. 4 (a) are plotted in Fig. 5. Pressure increases at each point until the end of the filling stage (0.46 sec), high pressure is maintained at every point of the part in the packing stage, and pressure drops gradually in the cooling stage.

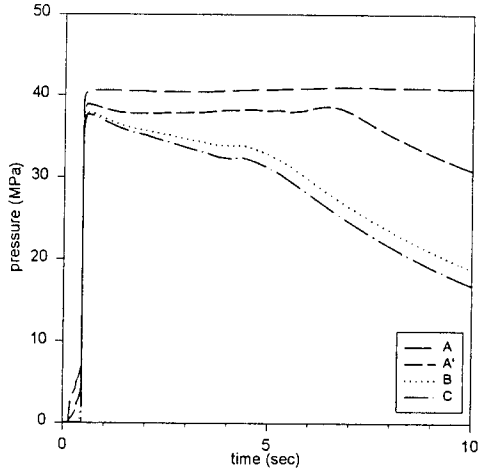

Fig. 5: Pressure variations predicted with respect to time at each point for mold A.

Figure 6 shows pressure and temperature distribution at the midplane between the centerplane and top wall of the cavity at 5.55 sec. Pressure decreases gradually as it is getting far from the gate and reaches a minimum value at the weld line (point C), while temperature shows a somewhat high value at the weld line due to the fountain effect and viscous heating. Temperature at the point near the gate (point A') is the highest due to the packing of the hot melt under high pressure in the packing stage.

Normal stress contours obtained from the stress analysis are shown in Fig. 7 (a). Overall distribution of the residual stress is similar to that of pressure (Fig. 6 (a)) except that the stress contours are similar to those of temperature (Fig. 6 (b)) near the gate. Since the residual stress analysis is based on the thermal stress analysis, distribution of the residual stress reflects the dependence of the thermal expansion coefficient upon not only temperature but also pressure. It can be identified from the stress contour that the residual stress is high at two points where the temperature is high, i. e., near the gate (point A') and at the weld line region where melt fronts reach lastly. Residual stresses around the gate where the cavity is filled early and cooled fast (right outside of point A') are low. Fig. 7 (b) shows the predicted deformed shape of the final product after it is cooled to room temperature. Displacements are magnified by a

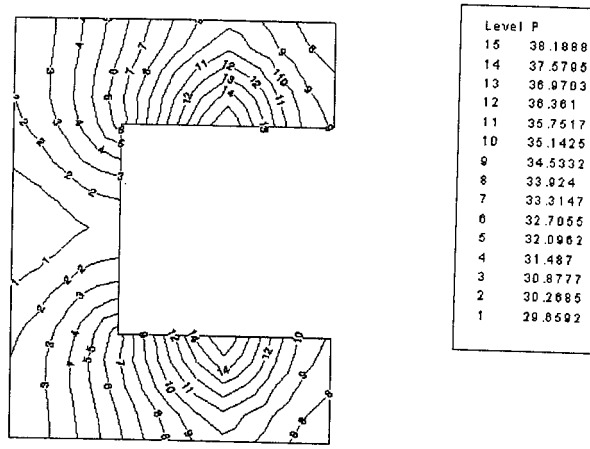

(a)

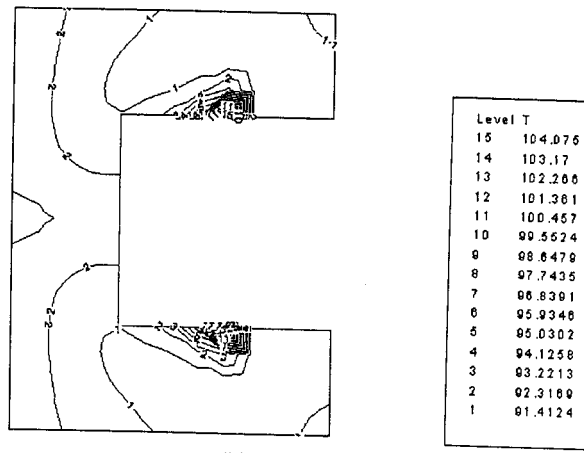

(b)

Fig. 6: Predicted contours of (a) pressure and (b) temperature at 5.55 sec (at postfilling stage) for mold A.

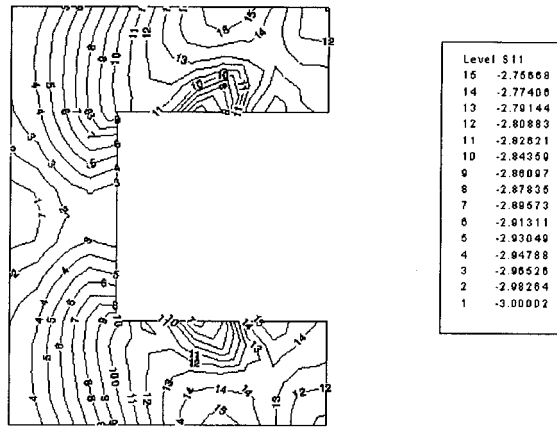

(a)

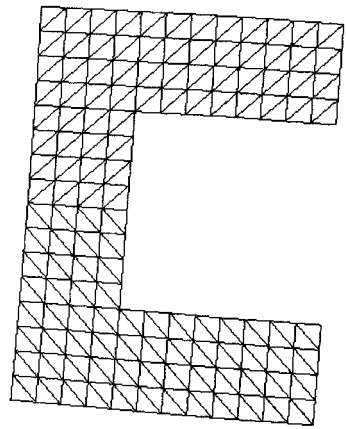

(b)

Fig. 7: (a) Predicted residual normal stress contours in x direction.
(b) Predicted deformed shape of the injection molded part for mold A.

factor of 10. The part has the largest deflection at the weld line and near the gate due to high temperature and high residual stresses.

Mold B

Figure 8 shows transient pressure profiles at specified positions shown in Fig. 4 (b).

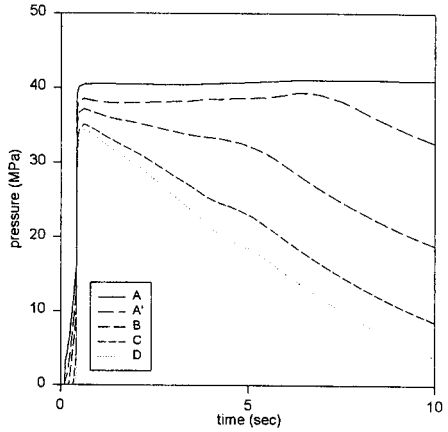

Fig. 8: Pressure variations predicted with respect to time at each point for mold B.

Pressure at the gate (point A) at the end of filling is at least two times higher than that of the previous case due to the difference in runner systems of mold A and B. As the cavity is filled through only one gate, flow path of the polymer melt becomes longer and pressure drop becomes larger. Thus, applied pressure should be increased to maintain a constant flow rate. It is shown that the pressure at locations far from the gate drops rapidly compared with the case of mold A during the postfilling stage. This rapid pressure drop is due to long flow path. Pressure and temperature contours for mold B are plotted in Fig. 9 which clearly shows that the pressure drop is larger than that of Fig. 6 (a).

Figure 10 (a) shows the distribution of σ_{11}, predicted by the residual stress analysis. The highest compressive residual stresses are observed around the gate area and at the end of the flow path. Figure 10 (b) shows the predicted deformed shape of the final part which undergoes large deflection around the gate because of high temperature and pressure changes.

Mold C

Figure 11 to 13 are results of the analysis for mold C. Figure 11 shows transient pressure profile at four positions shown in Fig. 4 (c). The longer the distance from the gate is, the

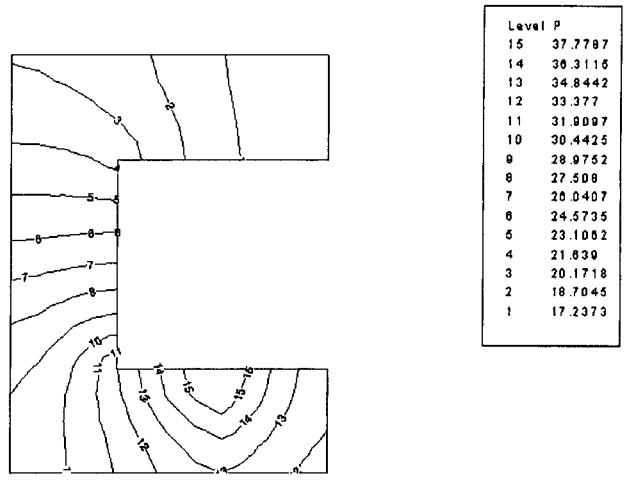

(a)

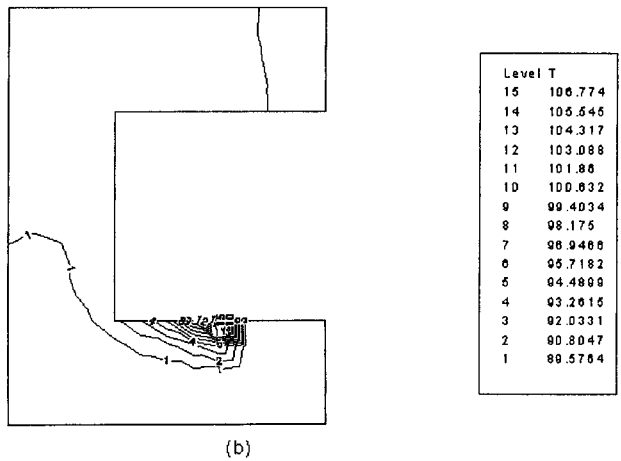

(b)

Fig. 9: Predicted contours of (a) pressure and (b) temperature at 5.71 sec (at postfilling stage) for mold B.

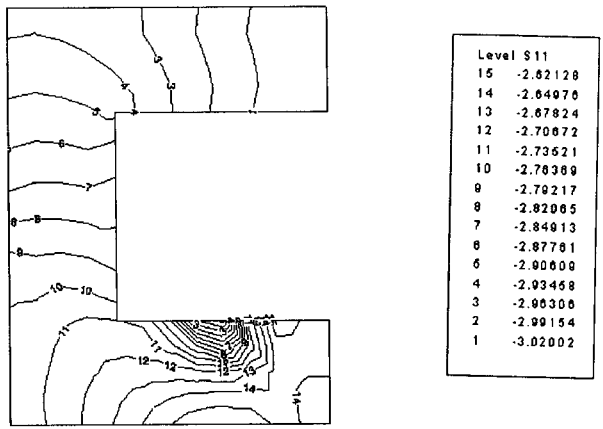

(a)

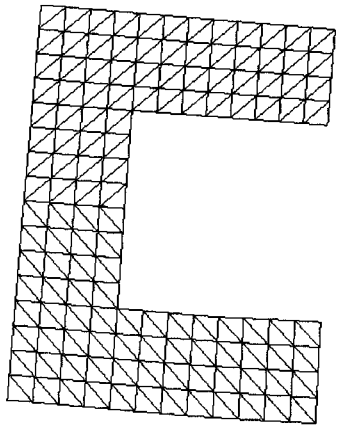

(b)

Fig. 10: (a) Predicted residual normal stress contours in x direction.
(b) Predicted deformed shape of the injection molded part for mold B.

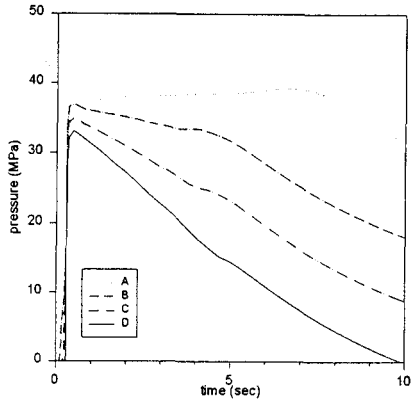

Fig. 11: Pressure variations predicted with respect to time at each point for mold C.

larger the pressure drop is as in the two previous cases. Pressure and temperature contours are plotted in Fig. 12 in the postfilling stages at 5.28 seconds.

As described in Fig. 13 (a), the longer the distance from the gate is, the larger the magnitude of the residual stress becomes. Its distribution is also similar to the distribution of pressure. It is observed in Fig. 13 (b) that the predicted residual stress field affects the deformed shape of the final part. It is noticed that large shrinkage occurs at the end of the flow path where the highest residual stress is induced.

Conclusions

A unified analysis of three stages of the injection molding process, which is essential not only for mold design such as gate locations, runner systems, and cooling systems but also for determination of processing conditions such as barrel temperature, mold wall temperature, clamping force, flow rate, etc., has been carried out in this study. A flow and thermal analysis considering all stages of injection molding is performed by using the compressible GHS model and thermally induced residual stresses are calculated from the data obtained as the result of the flow and thermal analysis.

Acknowloedgement

This work has been partially supported by the Korea Science and Engneering Foundation. The authors are grateful for the support.

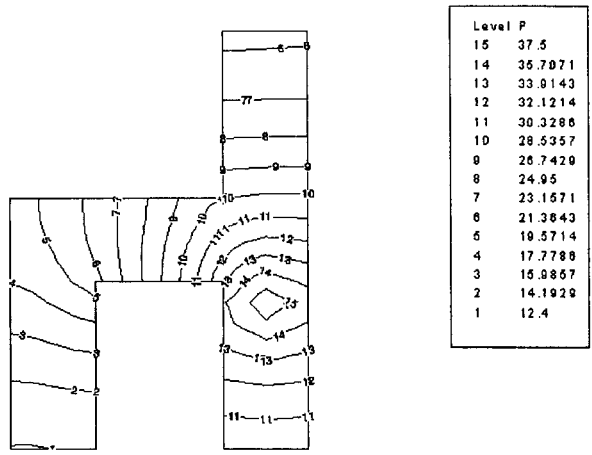

(a)

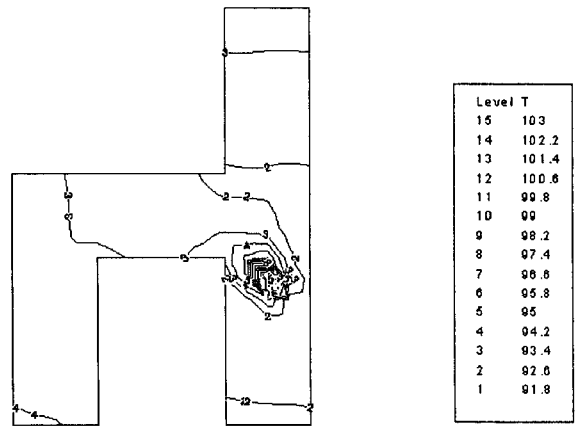

(b)

Fig. 12: Predicted contours of (a) pressure and (b) temperature at 5.28 sec (at postfilling stage) for mold C.

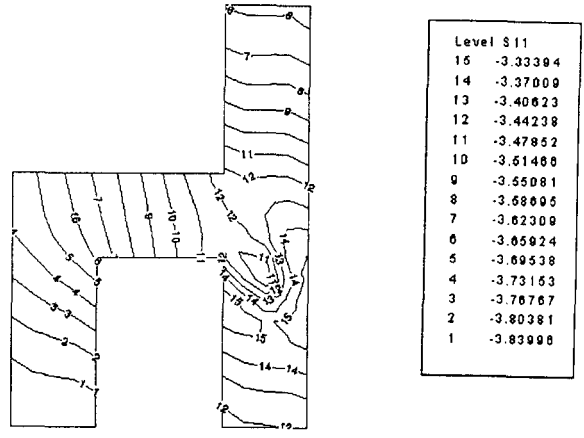

(a)

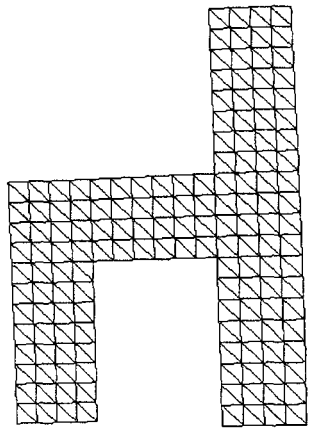

(b)

Fig. 13: (a) Predicted residual normal stress contours in x direction.
(b) Predicted deformed shape of the injection molded part for mold C.

References

1. C. A. Hieber, S. F. Shen, *J. Non-Newt. Fluid Mech.*, **7**, 1 (1980)
2. R. S. Spencer, G. D. Gilmour, *J. Appl. Phys.*, **21**, 523 (1950)
3. H. H. Chiang, C. A. Hieber, K. K. Wang, *Polym. Eng. Sci.*, **31**, 116 (1991)
4. H. H. Chiang, C. A. Hieber, K. K. Wang, *Polym. Eng. Sci.*, **31**, 125 (1991)
5. K. K. Kabanemi, A. Ait-Kadi, P. A. Tanguy, *Rheol. Acta.*, **34**, 97 (1995)
6. R. Wimberger-Friedl, *Prog. Polym. Sci.*, **20**, 369 (1995)
7. L. F. A. Douven, A. F. P. T. Baaijens, H. E. H. Meijer, *Prog. Polym. Sci.*, **20**, 403 (1995)
8. K. M. B. Jansen, G. Titomanlio, *Polym. Eng. Sci.*, **36**, 2029 (1996)
9. G. Titomanlio, K. M. B. Jansen, *Polym. Eng. Sci.*, **36**, 2041 (1996)
10. R. Y. Chang, B. D. Tsaur, *Polym. Eng. Sci.*, **35**, 1222 (1995)
11. S. K. Byon, *Ph. D Thesis*, KAIST, 1994, Taejon, Korea
12. C. A. Hieber, in: *Injection and Compression Molding Fundamentals*, A. I. Isayev (Eds.), Marcel Dekker, New York 1987, p. 61
13. B. S. Chen, W. H. Liu, *Polym. Eng. Sci.*, **34**, 835 (1994)